Chemical Engineering Journal 164 (2010) 106–114

Contents lists available at ScienceDirect

Chemical Engineering Journal

journal homepage: www.elsevier.com/locate/cej

Kinetic study of defluoridation of drinking water by electrocoagulation/electroflotation in a stirred tank reactor and in an external-loop airlift reactor

A.H. Essadki [a,*], B. Gourich [a], M. Azzi [b], Ch. Vial [c], H. Delmas [d]

[a] Ecole Supérieure de Technologie de Casablanca, BP 8012, Oasis Casablanca, Morocco
[b] Faculté des Sciences Aïn Chock, Laboratoire d'Electrochimie et Chimie de l'Environnement, BP 5366, Maarif, Casablanca, Morocco
[c] Clermont Université, ENSCCF, LGCB, 24 avenue des Landais, BP 206, 63174 Aubière Cedex, France
[d] Laboratoire de Génie Chimique, ENSIACET-INPT, 5 rue Paulin Talabot, 31106 Toulouse, France

ARTICLE INFO

Article history:
Received 7 October 2009
Received in revised form 12 August 2010
Accepted 17 August 2010

Keywords:
Defluoridation
Electrocoagulation
Electroflotation
Adsorption kinetics
Langmuir–Freundlich isotherm

ABSTRACT

A kinetic study of defluoridation of drinking water was carried out using the electrocoagulation/electroflotation process in two batch reactors of identical volume (20 L): a stirred tank reactor (STR) and an external-loop airlift reactor (ELALR). When the evolution of fluoride content was independent of stirring speed, experimental results showed that the kinetics of fluoride removal could be modelled using a variable-order-kinetic (VOK) approach coupled with a Langmuir–Freundlich adsorption model in the STR. Conversely, when mixing was less efficient, which is the case in the ELALR, experimental data could be fitted adequately only using a pseudo-first-order model. This constitutes however only an empirical approach based on a lumped parameter that accounts simultaneously for mass transfer, adsorption and electrochemical steps. In this case, only regression analysis could be used to establish a quantitative relationship between the kinetic constant and the operating conditions, such as current density and initial fluoride concentration.

1. Introduction

An excess amount of fluoride anions in drinking water has been known to cause adverse effects on human health. To prevent these harmful consequences, especially problems resulting from fluorosis, the World Health Organization (WHO) fixed the maximum acceptable concentration of fluoride anions in drinking water to 1.5 mg/L [1]. However, the fluoride content greatly exceeds the acceptable standards in many regions of Morocco. For example, on the plateau of Benguerir (centre of Morocco), water contains usually higher fluoride concentration than the standards for fluoride and may be sometimes brackish. In this region, fluoride contamination is essentially attributed to underground phosphate deposits; as a result, dental fluorosis is widespread among the population. A process that could efficiently remove fluoride anions from drinking water at relatively low capital and operating costs is therefore needed.

Various defluoridation processes have been developed to remove fluoride and improve the quality of drinking water, such as chemical precipitation and coagulation operation [2], ion exchange [3–5] and adsorption [6–8]. However, although these techniques have been widely applied, they present many limitations [9]. For example, the regeneration of adsorbents by chemical and thermal procedures is expensive, while chemical coagulation may induce a secondary pollution by using an excess of coagulants and generates usually large volumes of sludge. It is also worthy of note that the adsorption and ion exchange techniques are not able to remove fluoride at high concentration (higher than 5 mg/L). Recently, alternative defluoridation techniques based on membrane techniques [10–12] and electrocoagulation [13–17] have been developed, especially to remove fluoride from effluents containing between 5 and 20 mg/L F^-. If membrane processes are attractive, they are expensive in comparison to electrocoagulation. Electrocoagulation process appears therefore as a compromise between cost and efficiency.

In the recent years, some researchers have demonstrated that electrocoagulation (EC), using sacrificial aluminium electrodes, is an effective process for the defluoridation of drinking water and industrial wastewater [2,13,14,16,18]. For fluoride removal, EC seems to be able to replace chemical coagulation because it does not require a substantial investment, it produces less waste sludge and it improves the removal yield [19]. A literature survey indicates also that EC is an efficient process not only for the removal of fluoride anions, but also for the treatment of many types of wastes, such as other inorganic [20] or organic [21–23] pollutants from water. The application of EC induces various benefits

* Corresponding author. Tel.: +212 640338951; fax: +212 5 22252245.
E-mail address: essadki@est-uh2c.ac.ma (A.H. Essadki).

1385-8947/$ – see front matter © 2010 Elsevier B.V. All rights reserved.
doi:10.1016/j.cej.2010.08.037

Nomenclature

$[Al]_{tot}$	total aluminium concentration released from the anode (mol/L)
C_e	equilibrium fluoride concentration (mol/L)
D	diameter of the stirred tank reactor (m)
e	electrode gap (m)
EC	electrocoagulation
EF	electroflotation
ELALR	external-loop airlift reactor
F	Faraday's constant, $F = 96478$ (C/mol)
$[F^-]$	fluoride concentration (mol/L)
$[F^-]_0$	initial fluoride concentration (mol/L)
h	clear liquid height in the airlift reactor (m)
H	liquid height of the stirred tank reactor (m)
H_1, H_2, H_3, H_S	characteristic geometric dimensions of the airlift reactor (m)
h_D	dispersion height in the airlift reactor (m)
j	current density (A/m^2)
I	current (A)
k_L	Langmuir constant (L/mol)
k_F	Freundlich constant (L/mol)
k_{LF}	Langmuir–Freundlich constant (L/mol)$^{-n}$
k_1	pseudo-first-order rate constant (min^{-1})
K_{pred}	predicted k_1 value using Eq. (15) (min^{-1})
L	electrode height (m)
m	mass of flocs (g)
M	molar mass (g/mol)
n	Langmuir–Freundlich exponent (–)
p	Freundlich exponent (–)
pH_i	initial pH
q_e	mole of removed fluoride anions per mole Al(III) cations at equilibrium (mol/mol)
q_{max}	maximum amount of adsorbed fluoride anions per Al(III) cations (mol/mol)
q_{pred}	predicted q_e value (mol/mol)
R^2	regression/determination coefficient (–)
S	electrode surface (m^2)
STR	stirred tank reactor
t	time (min)
t_N	retention time required to achieve a desired $[F^-]$ value (min)
U	cell potential (V)
U_{Ld}	liquid velocity in the downcomer of the airlift reactor (m/s)
V	reactor volume (L)
VOK	variable-order-kinetic
Y	defluoridation yield (%)

Greek letters

ϕ_{Al}	efficiency of hydro-fluoroaluminum compound formation (%)
ϕ_c	current efficiency (%)
χ^2	Chi-square test for non-linear regression

in comparison to conventional treatments, including environmental compatibility, versatility, energy efficiency, safety, selectivity, amenability to automation and cost effectiveness [19,24,25]. This technique is based on the in situ formation of the coagulant as the sacrificial anode (usually aluminium or iron cations) corrodes due to an applied current. When aluminium is preferred, Al dissolves at the anode and hydrogen gas is released at the cathode. After dissolution, the aluminium cations are transformed into polymeric species [24] and form finally $Al(OH)_{3(s)}$ flocs, which depends on water properties (pH, alkalinity, co-existing anions, etc.). Floc separation can be obtained either by settling or flotation. In the last situation, electrocoagulation is denoted electroflotation (EF) and H_2 bubbles produced during electrolysis can carry flocs to the top of the reactor where they can be more easily concentrated, collected and removed.

The mechanism of the fluoride anion removal by EC was described and discussed by many authors [2,14,16,26]. It is however not fully understood because it includes actually several competing mechanisms involving soluble and insoluble fluoroaluminium complexes. Both the mechanisms of electrochemical coprecipitation of fluoroaluminium compounds and of adsorption on already formed fluoroaluminium particles have already been reported by Mameri et al. [14]. Zhu et al. [17] have also distinguished coprecipitation and adsorption on the electrode surface, denoted attachment, from the mechanisms involving the bulk. Their respective influence depends strongly on current density and operation time [17], but also on the water composition and properties, such as the presence of co-existing anions [13]. For example, Hu et al. [13] demonstrated that the presence of chloride anions together with the low electrode surface/reactor volume ratio S/V limits simultaneously adsorption and precipitation on electrodes. Conversely, Mameri et al. [14] reported that, for high ratio electrode S/V ratios, the direct coprecipitation of fluoroaluminium complexes near the electrodes prevailed. They showed that the rate of formation of these complexes was directly related to current density j up to an optimum value that depended on the S/V ratio. The authors concluded therefore that EC required S/V ratios higher than 10 m^2/m^3, with j values about 20 mA/m^2.

However, although the efficiency of the electrocoagulation process is known to be strongly dependent on the design and geometry of electrochemical reactors, it must be mentioned that most of the data of the literature was obtained using batch laboratory-scale EC cells. In laboratory experiments, only magnetic stirring was used and it was adjusted experimentally, while the separation step by flotation/sedimentation was not studied. The review of most of the literature concerning EC confirms a lack of dominant reactor design, although reactor design affects operational parameters including flow regime, floc formation, removal yield and flotation/settling characteristics [20]. Mollah et al. [24] described six typical configurations for industrial EC cells, but actually, the literature focuses mainly on electrode design [19,24] and electrode material [19] as the two aspects of EC configuration. Only recently, Hansen et al. [20] tested and compared three types of electrocoagulation reactors for the removal of arsenic. Among these three reactors, an internal-loop airlift reactor was studied. In comparison to internal-loop airlift reactors, external-loop airlift reactors (ELALR) offer the advantage to allow various designs of the separator section, which favours gas disengagement at the top of the reactor [27]. This is the reason why Essadki et al. [28] developed an application of EC/EF in an external-loop airlift reactor applied to the decolorization of textile dye wastewater. These authors demonstrated that good mixing conditions and complete flotation of the flocs were achieved using only the overall recirculation of the liquid phase induced by the electrochemically generated gas bubbles of hydrogen from the cathode. The main weakness of this reactor is however that the overall liquid circulation velocity must remain low in order to avoid floc erosion or recirculation in the downcomer, which implies that mixing is less efficient, for example, than in conventional turbulent flow reactors [20]. The principle of a co-current gas–liquid flow induced by electrogenerated H_2 bubbles has however been retained to design a reactor dedicated to decolorization using electroflotation [29].

The same external-loop airlift reactor was used first to investigate defluoridation of drinking water by EF/EF [30], and then in a comparative study in which the removal yield in an ELALR was

compared to that in a stirred tank reactor (STR) [31] These works highlighted that the ELALR did not require additional mechanical power for mixing, as this was induced only by the electrogenerated gas phase. Flotation was complete in the ELALR because the sludge was less eroded by mechanical stirring and could be recovered more rapidly than in a STR in which recovery had to be achieved both by flotation and settling. In [31], further information was also obtained on the mechanisms of defluoridation, especially as a function of the initial pH. The measurement of the soluble aluminium species in water by the inductive coupled plasma technique and the analysis of the sludge formed at two initial pH values (4 and 7) by scanning electronic microscope coupled with EDX elemental analysis demonstrated that the coprecipitation of Al–F complexes due to pH change in the reactor was more efficient than ion exchange/adsorption on $Al(OH)_3$ particles formed directly in the region of the electrode when the initial pH was 4, whereas the minimum solubility of Al around pH 7 favoured the formation of $Al(OH)_3$ particles followed by the adsorption and ion exchange with F^- anion in the reactor when the initial pH was 7. Thus, the optimum initial pH was found close to 4, although the maximum amount of the sludge was obtained for an initial pH close to 7 [31].

In [31], the authors demonstrated also that both the STR and the ELALR presented nearly the same ability in terms of fluoride removal yield when the aim was to achieve the legal standards, i.e. less than 1.5 mg/L residual fluoride in water, with similar energy and Al mass requirements, when Al dissolution by electrolysis remained the limiting step of defluoridation, i.e. when $j \leq 12\ mA/cm^2$. The removal yield was however higher in the STR at the beginning of the electrolysis, whereas similar values were usually achieved after 15 min operation. The objective of this work is, therefore, to develop a modelling approach able to simulate EC/EF data and to better understand the mechanisms that govern defluoridation and can explain the discrepancies between both reactors. The respective influences of current density, initial pH values, water conductivity and initial fluoride concentration are investigated.

2. Materials and methods

The defluoridation of drinking water was studied in two types of electrocoagulation reactors working under batch conditions: an electrochemical, mechanically stirred reactor (STR) and an external-loop airlift reactor (ELALR). Both of them had the same clear liquid volume $V = 20$ L. The ELALR (Fig. 1) is an innovative reactor for EC/EF process: its geometrical details and its operating conditions were described previously [28] and will only be reminded in this work: the diameters of the riser and the downcomer were 94 and 50 mm, respectively; both sections were 147 cm height ($H_2 + H_3$) and were connected at the bottom by a junction of 50 mm diameter and at the top by a rectangular gas separator (or gas disengagement section) of $H_S = 20$ cm height; at the bottom, the curvature radius of the two elbows was 12.5 cm in order to minimize friction and avoid any dead zone; the distance between the vertical axes of the riser and the downcomer was 675 mm, which limited the recirculation of bubbles and particles from the riser into the downcomer. The desired liquid volume corresponded to a clear liquid level (h) of 14 cm in the separator section. Contrary to conventional operation in airlift reactors, no gas phase was sparged at the bottom of the riser; only electrolytic gases (H_2 microbubbles) induced the overall liquid recirculation resulting from the density difference between the fluids in the riser and the downcomer [27].

The STR consisted of a dished-bottom cylindrical tank of internal diameter $D = 23$ cm and ratio $H/D = 2.4$ equipped with a two-blade marine propeller of 6 cm diameter placed 6 cm from the bottom in order to avoid settling and favour EC/EF, as in the ELALR. In the STR, the anode and cathode were both flat aluminium electrodes of

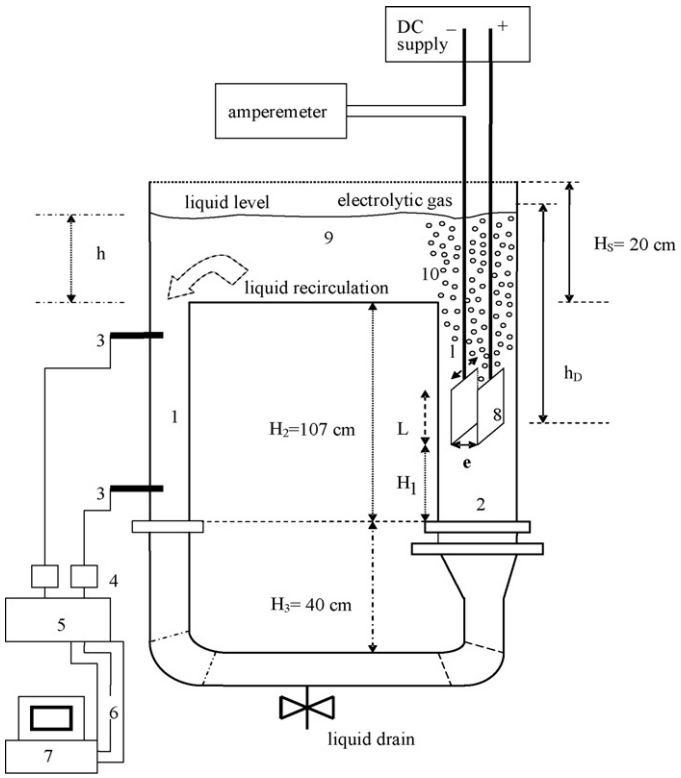

Fig. 1. External-loop airlift reactor (1: downcomer section; 2: riser section; 3: conductivity probes; 4: conductimeter; 5: analog output/input terminal panel (UEI-AC-1585-1); 6: 50-way ribbon cable kit; 7: data acquisition system; 8: electrodes; 9: separator; 10: electrochemically generated bubbles).

rectangular shape (250 mm × 70 mm × 1 mm). The effective area of the anode was $S = 175\ cm^2$; the electrodes were vertically centred between the bottom of the reactor and the liquid level, and placed 6.5 cm from the shaft of the impeller to maintain an equal distance between the wall and the middle of the blades of the impeller. The same electrodes were used in the ELALR and the distance between electrodes was $e = 20$ mm in both reactors. Further details on the role of the axial position of the electrodes are available in a previous work on the decolorization of textile dye wastewater in the same setup [28]. Previous results showed that flocs erosion could be prevented when the liquid velocity in the downcomer U_{Ld} was lower than 8–9 cm/s in the presence of dispersive dyes [28].

In both reactors, all experiments were conducted at room temperature ($20 \pm 1\ ^\circ C$) and atmospheric pressure. The desired potential (U) between electrodes was monitored by a digital DC power supply (Didalab, France) and current was measured by an amperemeter. Current density values (j) between 2.8 and $17\ mA/cm^2$ were investigated, which corresponded to current ($I = j \cdot S$) in the range 0.5–3 A. Conductivity and pH were measured using a CD810 conductimeter (Radiometer Analytical, France) and a ProfilLine pH197i pHmeter (WTW, Germany). Samples were filtered and the concentration measurements of the remaining fluoride anions were determined in the solution by means of a combined selective fluoride electrode ISEC301F and a PhM240 ionmeter (Radiometer Analytical, France), using the addition of a TISAB II buffer solution to prevent interference from other ions. pH could be adjusted by a minute addition of either HCl or NaOH aqueous solutions. In this work, the initial pH (pH_i) was fixed at 7.4; water conductivity could also be adjusted using the addition of sodium chloride (Carlo Erba Réactifs, France). The evolution of turbidity over time was measured on non-filtered samples in order to follow floc separation by flotation using a 550IR turbidimeter (WTW, Germany). Experiments were carried out using typical Casablanca

Table 1
Typical properties of Casablanca drinking water.

pH	7.85
Alkalinity (mg/L $CaCO_3$)	150
Total hardness (mg/L)	350
Turbidity (NTU)	0.15
Chloride anions (mg/L)	392

drinking water (Table 1) in which an initial fluoride concentration $[F^-]_0$ between 10 and 20 mg/L was obtained by adding sodium fluoride NaF (Carlo Erba Réactifs, France). The yield of fluoride removal could be calculated as follows:

$$Y\ (\%) = 100 \cdot \frac{[F^-]_0 - [F^-]}{[F^-]_0} \quad (1)$$

using the initial fluoride concentration $[F^-]_0$ and the remaining fluoride concentration $[F^-]$ that was measured over time by means of the combined selective electrode.

3. Results and discussion

3.1. Effect of stirring speed in the STR

As EC/EF operation was conducted in the intensiostat mode, the release of aluminium cations from the electrodes was not dependent on mixing and could not be influenced by mass transfer limitations. In the STR, no significant decrease of voltage U was reported as a function of the increase of the stirring speed of the impeller in the range studied (50–200 rpm). As a result, at pH 7.4, stirring speed acted mainly on the mixing of $Al(OH)_3$ particles formed in the region of the electrodes into the bulk and on the apparent adsorption kinetics of fluoride anions, especially when this was limited by external mass transfer [31]. The advantage of the STR was that current density and mixing could be controlled independently, which was not the case in the ELALR [28]. The key influence of stirring speed on fluoride removal in the STR had already been studied experimentally in [31]; data showed that the yield of fluoride removal became nearly independent of stirring speed when this approached 200 rpm. This is the reason why experimental data from the STR in the following sections have always been obtained at 200 rpm, except otherwise mentioned. However, the experimental results of [31] at several stirring speeds can be revisited on the basis of Fig. 2. In this figure, current density, initial pH and conductivity were fixed at 17 mA/cm^2, 7.4 and 2.4 mS/cm, respectively. If the governing mechanism of EC followed a first-order kinetics, the evolution of the function $Ln([F^-]_0/[F^-])$ vs. time should be a straight line in Fig. 2. However, only the curve corresponding to 50 rpm presents a linear shape in this figure, after a time lag of 4 min that can be attributed to poor mixing conditions. At 100 rpm, two linear regions could be identified in Fig. 2. Nevertheless, this behaviour seemed only to be a degenerated form of the more complex trends observed at 200 and 400 rpm in which these two regions still appeared, but both exhibiting a non-linear shape.

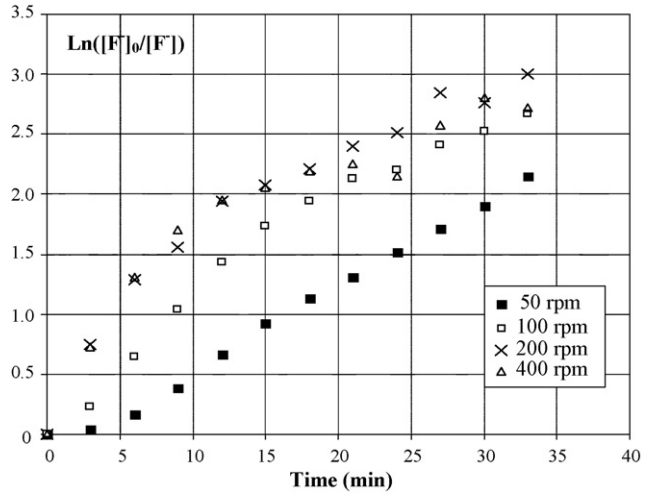

Fig. 2. Influence of stirring speed on the evolution of fluoride anion concentration in the STR ($[F^-]_0$ = 15 mg/L, pH_i 7.4, κ = 2.4 mS/cm).

These results do not match most of those reported in the literature. For example, Mameri et al. [14] showed that the formation of fluoroaluminium complexes and the precipitation of $Al(OH)_3$ followed second- and first-order kinetics, respectively. In addition, external mass transfer limitations correspond to a first-order process; similarly, the internal mass transfer limitations usually follow a first- or second-order kinetics in adsorbents, but should be insensitive to stirring speed. However, it must be reminded that most data from the literature was obtained in electrolytic cells of about 1 L volume in which mixing was ensured only by magnetic stirring with high electrode surfaces that favoured dead zones. Even though a first-order kinetics was expected at pH 7.4 at high stirring speed in the STR, it seems that a first-order mechanism prevailed only when the operation was limited by mixing at low stirring speed, and more probably by the external mass transfer during the adsorption of fluoride anions onto $Al(OH)_3$ particles. At higher stirring speed, other mechanisms probably limited fluoride removal. In this case, a possible explanation is that the defluoridation rate was first limited by adsorption, in particular by the maximum amount of fluoride anions on the adsorbent at the beginning of EC/EF. Indeed, contrary to conventional batch adsorption processes in which adsorption capacity and pollution concentration are maximum at the same time, the amount of insoluble $Al(OH)_3$ particles starts from zero at the beginning of EC/EF, i.e. when $[F^-]$ is maximum. This is the reason why the adsorption isotherm of fluoride anions on $Al(OH)_3$ flocs will be studied in the next section.

3.2. Adsorption isotherms

Experimental isotherms constitute a useful tool for describing the adsorption capacity of a specific adsorbent. Moreover, the isotherms play a vital role for the analysis and design of adsorption systems, as well as for the modelling and simulation of adsorption processes. Many theoretical models have been developed in the literature so as to describe the experimental data corresponding to adsorption isotherms, but two of them are mainly used for describing adsorption in the liquid phase: the Langmuir and the Freundlich model. A combined version of these two models, the Langmuir–Freundlich equation, is also sometimes used to fit experimental data [32]. The mathematical forms of these isotherms are summarized below:

$$\text{Langmuir} \quad q_e = q_{max} \cdot \frac{k_L C_e}{1 + k_L C_e} \quad (2)$$

$$\text{Freundlich} \quad q_e = k_F \cdot C_e^{1/p} \quad (3)$$

$$\text{Langmuir–Freundlich} \quad q_e = q_{max} \cdot \frac{k_{LF} C_e^n}{1 + k_{LF} C_e^n} \quad (4)$$

where q_e is the molar amount of removed fluoride anions per mole of Al(III) cations in $Al(OH)_3$ at equilibrium and C_e is the equilibrium fluoride concentration in water, q_{max} is the adsorption capacity of fluoride anions per mole of Al(III) cations, k_L is the Langmuir constant that measures the affinity between the fluoride anions and the adsorbent, k_F and p are the Freundlich parameters, and k_{LF} and n are the Langmuir–Freundlich parameters.

For the determination of the adsorption isotherm, $Al(OH)_3$ flocs were produced by electrolysis in the STR using the same

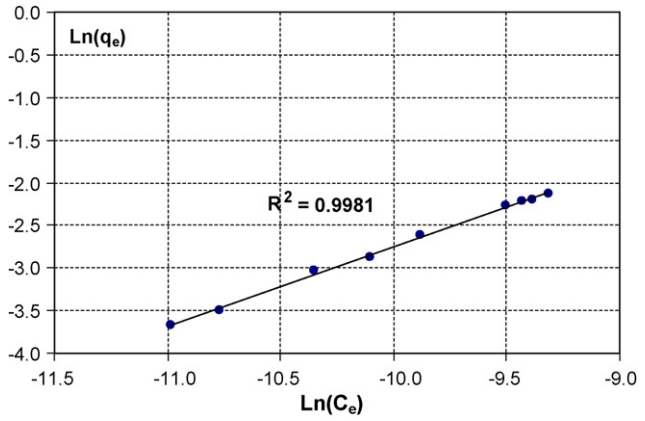

Fig. 3. Characteristic linear plot of Freundlich isotherm for pH_i 7, $[F^-]_0$ = 15 mg/L, κ = 7.5 mS/cm, j = 17.1 mA/cm^2.

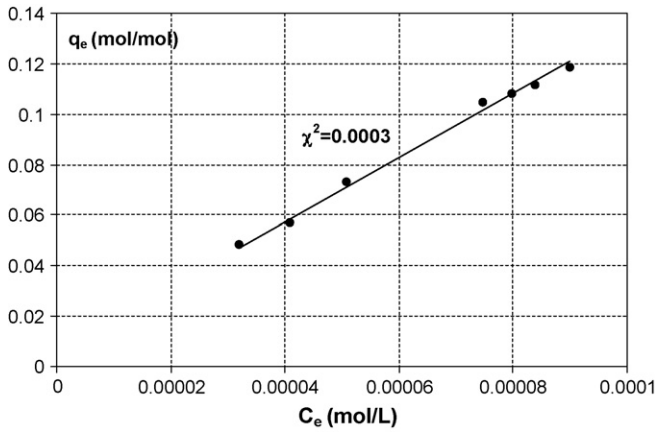

Fig. 4. Comparison of predicted q_{pred} vs. experimental q_e values using Langmuir–Freundlich isotherm for pH_i 7, $[F^-]_0$ = 15 mg/L, κ = 7.5 mS/cm, j = 17.1 mA/cm^2.

experimental methodology as described for EC/EF, but without fluoride anions in water (200 rpm, pH_i 7.0, j = 17.1 mA/cm^2 and κ = 7.5 mS/cm). These flocs were recovered, dried, weighed and analyzed, which lead to the weight of $Al(OH)_3$ in flocs. Then, a known quantity of dried flocs, between 5 and 13 g was brought into contact with fluoride solutions of concentrations between 0.33 and 1.05 mM. The experiments were conducted in the STR, at 200 rpm, pH_i 7.0 and κ = 7.5 mS/cm. After 4 h, the equilibrium fluoride concentration C_e was measured using the specific electrode and q_e was deduced as follows:

$$q_e = V \cdot \frac{[F^-]_0 - C_e}{m_{Al(OH)_3}} \cdot M_{Al(OH)_3} \quad (5)$$

In Eq. (5), m and M are the initial mass and the molecular weight of $Al(OH)_3$, respectively.

Experimental data was confronted to the three models summarized by Eqs. (2)–(4). For Langmuir and Freundlich isotherms, the unknown parameters q_{max} and k_L can be deduced from a linear regression after transformation of Eqs. (2) and (3) into linear forms; for Langmuir isotherm, several linear forms have been proposed [32], among which the two most popular are expressed as:

$$\frac{C_e}{q_e} = \frac{1}{q_{max}k_L} + \frac{C_e}{q_{max}} \quad \left(\frac{C_e}{q_e} \text{ is plotted vs. } C_e\right) \quad (6)$$

$$\frac{1}{q_e} = \frac{1}{q_{max}k_L} \cdot \frac{1}{C_e} + \frac{1}{q_{max}} \quad \left(\frac{1}{q_e} \text{ is plotted vs. } \frac{1}{C_e}\right) \quad (7)$$

For Freundlich isotherm, k_F and p were estimated using the $Ln(q_e)$ vs. $Ln(C_e)$ plot. For the combined model of Langmuir–Freundlich isotherm, the three parameters (q_{max}, k_{LF} and n) were adjusted by non-linear optimization methods. For comparison purpose, Langmuir and Freundlich isotherms were also tested on the basis of non-linear methods.

Figs. 3 and 4 show that the Freundlich and Langmuir–Freundlich isotherms fit adequately experimental data, which is confirmed by the regression coefficients added in Fig. 3 and by the Chi-square (or goodness-of-fit) test χ^2 for the non-linear regression in Fig. 4; χ^2 can be estimated using Eq. (8) that compares experimental (q_e) and predicted (q_{pred}) values at the same C_e:

$$\chi^2 = \sum \frac{[q_e(C_e) - q_{pred}(C_e)]^2}{q_{pred}(C_e)} \quad (8)$$

Small χ^2 values indicate that experimental data and predictions are close and, consequently, validate the goodness-of-fit. Finally, Fig. 5 confirms that the Langmuir isotherm may also describe experimental data, although the regression coefficient is clearly improved using Eq. (3) in Fig. 5b than Eq. (2) in Fig. 5a.

Table 2 summarizes the estimated parameters of the three models. For linear regressions, the error on the estimation of these parameters was deduced using Student statistics. This shows that the two linear forms for the Langmuir model provided similar estimations in Table 2, despite the difference in regression coefficients between the two plots in Fig. 5. A better reduction of χ^2 was however achieved using non-linear methods, although the goodness-of-fit test could never be rejected with 95% confidence level, as $\chi^2 < 12.6$ for Langmuir–Freundlich fitting (three adjustable parameters) and $\chi^2 < 14.1$ for the others with two adjustable parameters. More accurate estimations were however obtained using the Freundlich and the Langmuir–Freundlich isotherms in Table 2, but the Langmuir–Freundlich isotherm is probably over-

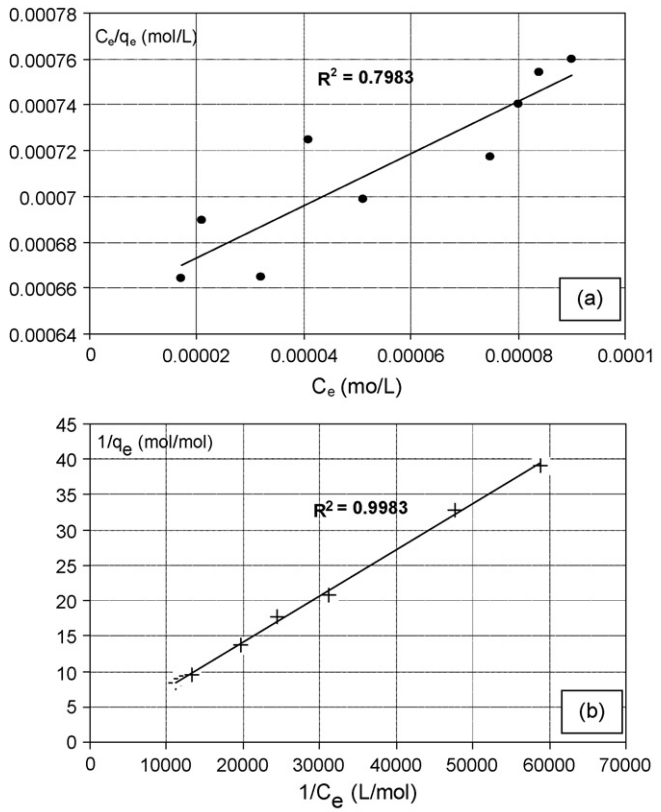

Fig. 5. Characteristic linear plots of Langmuir isotherm for pH_i 7, $[F^-]_0$ = 15 mg/L, κ = 7.5 mS/cm, j = 17.1 mA/cm^2: (a) C_e/q_e vs. C_e (Eq. (2)); (b) $1/q_e$ vs. $1/C_e$ (Eq. (3)).

Table 2
Comparison of adsorption parameters deduced from the experimental adsorption isotherm using different models and methods to fit the data.

	Langmuir (Eq. (2))	Langmuir (Eq. (3))	Langmuir (optimization)	Freundlich (linear)	Freundlich (optimization)	Langmuir–Freundlich
q_{max} (mg/g)	0.9 ± 0.4	0.9 ± 0.5	0.9	–	–	0.90
k_L (L/mol) k_{LF} (L/mol)$^{-n}$	1300 ± 700	1300 ± 700	1650	–	–	1675
k_F	–	–	–	700 ± 40	695	–
$1/p$	–	–	–	0.93 ± 0.04	0.93	–
n	–	–	–	–	–	1.01
R^2	0.798	0.998	–	0.998	–	–
χ^2	0.03	0.03	0.0002	0.0003	0.0003	0.0003

parametrized in the present case, as it includes three adjustable parameters. Table 2 shows finally that the best compromise was obtained using the Freundlich isotherm, as it provided small χ^2 values with only two adjustable parameters and was nearly insensitive to the fitting procedure, with an exponent $1/p$ close to 1.

3.3. Analysis of defluoridation kinetics

3.3.1. Applicability of the variable-order-kinetic (VOK) approach to the STR

The kinetics of the defluoridation experiments by electrocoagulation needs to be examined for estimating the time required for defluoridation. As mentioned in Section 3.1, a first-order kinetic law is the most common in the literature [14,18]; however, the first-order kinetic constant was reported to depend on current density, electrode gap, pH_i and even initial fluoride concentration [18]. This means that data from the literature corresponded to an empirical pseudo-first-order process, as the removal yield Y should be independent of $[F^-]_0$ for any first-order mechanism of kinetic constant k_1 (Eq. (9)):

$$Y = 1 - \exp(-k_1 \cdot t) \tag{9}$$

However, even a pseudo-first-order approach does not fit the experimental data of [31] for the STR when stirring speed is above 100 rpm (Fig. 2).

An alternative approach was suggested by Hu et al. [26]; these authors developed a variable-order-kinetic model (VOK) in which defluoridation could be limited by the capacity of the adsorbent. This presents the advantage to account for the adsorption phenomenon in order to estimate the time required for defluoridation by EC. As a result, the defluoridation rate in the VOK approach is assumed to be proportional to the kinetics of aluminium release, expressed as the total aluminium concentration in solution $[Al]_{tot}$, which gives access to the amount of adsorbent available at ay time. Consequently, the fluoride removal rate can be expressed as follows:

$$-\frac{d[F^-]}{dt} = \phi_{Al} \cdot q_e \cdot \frac{d[Al]_{tot}}{dt} \tag{10}$$

where ϕ_{Al} is the efficiency of the formation of fluoroaluminium compounds. The rate of Al release from the electrodes can be deduced from Faraday's law:

$$\frac{d[Al]_{tot}}{dt} = \phi_c \frac{I}{3F \cdot V} \tag{11}$$

where ϕ_c is the faradic yield, I is the applied current, F Faraday's constant and V is the volume of the reactor.

Hu et al. [26] limited their VOK model to the particular situation in which q_e could be fitted using Langmuir isotherm. This approach was tested, but again, it did not fit the experimental data of [31]. It must be reminded, that Hu et al. [26], as Emamjomeh and Sivakumar [18], used small laboratory electrolytic cells with magnetic stirring, whereas a 20 L mechanically stirred reactor was used in this work. This may explain why their and our results do not agree. Similar trends were, however, observed when the Freundlich isotherm was introduced in Eq. (10), even though it was retained in Section 3.2: neither Langmuir, nor Freundlich isotherms were able to represent adequately the experimental results. Another difference with the literature was that the S/V ratio was lower both in the ELALR and the STR (0.875 m^2/m^3) than in the conventional EC cells in which the S/V ratio ranged between 10 and 40 m^2/m^3 [14,26]. At high S/V ratios, Zhu et al. [17] demonstrated that fluoride adsorption/attachment on the electrode was primarily responsible for defluoridation efficiency, while other mechanisms played only a secondary role. Conversely, fluoride removal by attachment on the electrodes was negligible when S/V = 0.875 m^2/m^3 and the prevailing mechanisms were in the bulk, i.e. the simultaneous formation of soluble fluoroaluminium compounds, their coprecipitation with $Al(OH)_3$ and the simultaneous adsorption of fluoride anions on the insoluble species. This may also explain why the conventional isotherms are not able to fit experimental data, as the quantity of adsorbent was close to zero at the beginning of EC in the STR, while it was not negligible due to electrode attachment at high S/V ratio.

As a result, only the VOK model based on the Langmuir–Freundlich isotherm will be developed in this section. Combining Eqs. (10) and (11) with Eq. (4) gives:

$$-\frac{d[F^-]}{dt} = \phi_{Al} \cdot \phi_c \frac{I}{3F \cdot V} \cdot \frac{q_{max} \cdot k_{LF} \cdot [F^-]^n}{1 + k_{LF} \cdot [F^-]^n} \tag{12}$$

Using Eq. (12), the pseudo-first-order rate constant can be obtained and expressed as follows:

$$k_1 = \phi_{Al} \cdot \phi_c \frac{I}{3F \cdot V} \cdot \frac{q_{max} \cdot k_{LF} \cdot [F^-]^{n-1}}{1 + k_{LF} \cdot [F^-]^n} \tag{13}$$

The retention time (t_N) required in order to achieve an objective in terms of residual fluoride concentration $[F^-]$ can be determined by integrating Eq. (12):

$$t_N = \frac{3F \cdot V}{\phi_c \phi_{Al} \cdot I \cdot q_{max}} \left[([F^-]_0 - [F^-]) + \frac{1}{k_{LF}(1-n)} ([F^-]_0^{1-n} - [F^-]^{1-n}) \right] \tag{14}$$

Eqs. (12) and (14) predict that the defluoridation rate and $1/t_N$ should be proportional to current density I, provided the faradic yield ϕ_c does not vary with I, which is not ascertained for aluminium electrodes. Eq. (12) also corresponds to an apparent zeroth-order when $k_{LF}[F^-] \gg 1$ (limitation due to adsorption capacity) and to an apparent first-order when $k_{LF}[F^-] \ll 1$ (limitation due to low fluoride content).

The VOK model combined to Langmuir–Freundlich isotherm will be confronted to the experimental data obtained at pH_i 7.4 of [31], as a function of current density (Section 3.3.1.1) and initial fluoride concentration (Section 3.3.1.2). This pH_i value was shown to maximize sludge formation [31], which is interesting for analyzing the influence of adsorption.

3.3.1.1. Effect of current density. Fig. 6 shows the effect of the current density on the evolution of the fluoride concentration in the STR during EC. The initial pH and initial fluoride concentration

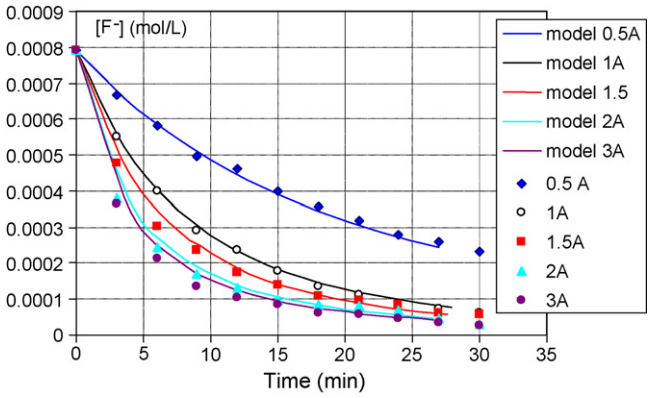

Fig. 6. Evolution of fluoride ion concentration during EC: influence of current (pH_i 7.4, κ = 7.5 mS/cm, $[F^-]_0$ = 15 mg/L) in the STR and comparison with the predictions of the VOK model.

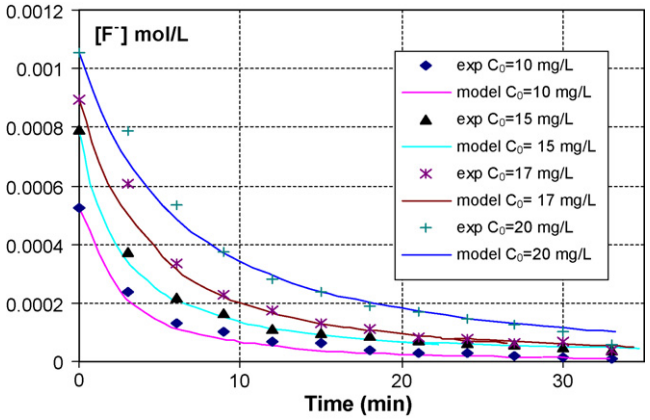

Fig. 7. Evolution of fluoride ion concentration during EC: influence of the initial fluoride concentration C_0 (pH_i 7.4, κ = 6.1 mS/cm, j = 17.1 mA/cm^2) on experimental data (exp) in the STR and comparison with the predictions of the VOK model.

were fixed at 7.4 and 15 mg/L, i.e. 0.8 mmol/L, respectively. Fig. 6 also displays the predictions corresponding to the VOK model after optimization of the adjustable parameters q_{max}, k_{LF} and n. These parameters are summarized in Table 3, which shows that they depend only slightly on current density, as expected. Two conclusions can be made when Table 2 and Table 3 are compared. First, k_{LF} keeps nearly the same value. Secondly, q_{max} is far higher when estimated from EC experiments, which probably stems from a change of mechanism: in isotherm measurements (Section 3.1), adsorption proceeds on already formed $Al(OH)_3$ particles; conversely, fluoride is progressively introduced in flocs during their formation in EC operation, which can also be accelerated by the incorporation of fluoroaluminium complexes. As a result, the maximum amount of fluoride that can be recovered is far higher in EC, which is confirmed by an exponent n higher than 1 (about 1.5) that indicates a cooperative adsorption mechanism. Finally, the applicability of the VOK model coupled with Langmuir–Freundlich isotherm in the STR is also assessed by the fact that it was established for operation times up to 24 min, whereas the simulations of Hu et al. [26] did not exceed 9 min.

As a conclusion, the model and the experiments highlight that current density plays the key role, as it governs the amount of coagulant produced in situ vs. time. The kinetics of fluoride was not exactly proportional to current in the experiments when I is higher than 1 A. Consequently, the simulations show clearly that EC was limited by the rate of aluminium released only for I = 0.5 A. This explains why the behaviour at j = 2.85 mA/cm^2 could be explained by a weak charge loading in this case (0.47 F/m^3) in [31]. For higher current, the curves less differ, especially after 15 min operation when the low concentration of fluoride anions constituted the only limiting step of defluoridation, i.e. when $k_{LF}[F^-] \ll 1$. This shows that about 0.9 F/m^3 is needed to optimize the removal yield of fluoride anions. A comparison with the data of Shen et al. [16] shows that they needed 5–6 F/m^3 to achieve 1.5 mg/L with $[F^-]_0$ between 10 and 15 mg/L, which emphasizes the high effectiveness of the STR.

Table 3
Parameters adjusted from the experimental data of the STR using the VOK model coupled with Langmuir–Freundlich isotherm: influence of current density (pH_i 7.4, κ = 6.1 mS/cm, $[F^-]_0$ = 15 mg/L).

j (mA/cm^2)	n	k_{LF} (L/mol)$^{-n}$	q_{max} (mol/mol)	χ^2
2.8	1.52	1500	300	0.34
5.7	1.49	1500	300	0.39
8.6	1.50	1500	300	0.31
11.4	1.52	1500	300	0.81
17.1	1.55	1500	300	0.34

3.3.1.2. Effect of initial concentration. The experiments conducted at various initial fluoride concentrations from 10 to 20 mg/L were confronted to the VOK model, keeping all other conditions identical (j = 17.1 mA/cm^2, pH_i 7.4, κ = 7.5 mS/cm). For the STR, Fig. 7 shows that the rate of defluoridation was significantly influenced by the initial concentration of fluoride. The time required to achieve a defined removal yield Y increased when the initial concentration increased. As in Figs. 6 and 7 compares also experimental data with the simulations using the VOK model for various initial fluoride concentrations: a good fitting of the experimental data was obtained using Langmuir–Freundlich isotherm. The estimated parameters are summarized in Table 4. This table shows that k_{LF} and q_{max} did not vary significantly with $[F^-]_0$ and did not differ significantly from the values of Table 3. However, the exponent n increased slightly with the initial fluoride concentration and the values of χ^2 were higher than in Table 3, although the goodness-of-fit test was never rejected. Consequently, it seems that the kinetics of adsorption changes as a function of $[F^-]_0$ and that removal fluoride becomes more difficult when the initial concentration increases, as $[F^-]^n$ decreases when $n > 1$ increases for $[F^-] < < 1$. However, the applicability of the VOK model coupled with Langmuir–Freundlich isotherm in the STR is also assessed, as the variability of n remains limited; the model can therefore be used to predict the effectiveness of EC in the STR.

3.3.2. Applicability of the pseudo-first-order empirical kinetics in the ELALR

Contrary to the STR (Fig. 2), Fig. 8 shows that a first-order kinetics (Eq. (9)) is able to model adequately the experimental results of the ELALR in which mixing is less efficient than in the STR. Fig. 8 shows, indeed, that $-\mathrm{Ln}(1-Y)$ varies proportionally with time, which indicates that the kinetics of defluoridation follows an exponential decrease with time for a fixed initial fluoride concentration, pH_i and conductivity of 15 mg/L, 7.4 and 2.4 mS/cm, respectively. However, the kinetic constant k_1 increased from 0.052 to 0.117 min^{-1} when current density increased from 2.85 to 17.1 mA/cm^2. This result is

Table 4
Parameters adjusted from the experimental data of the STR using the VOK model coupled with Langmuir–Freundlich isotherm: influence of initial fluoride concentration (pH_i 7.4, κ = 6.1 mS/cm, j = 17.1 mA/cm^2).

$[F^-]_0$ (mg/L)	n	k_{LF} (L/mol)$^{-n}$	q_{max} (mol/mol)	χ^2
10	1.50	1500	300	1.3
15	1.57	1500	300	1.3
17	1.59	1500	300	1.3
20	1.64	1500	300	1.1

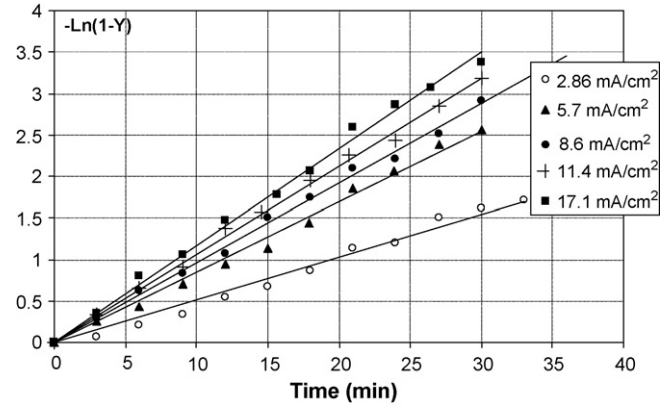

Fig. 8. Determination of the kinetic constant of defluoridation in the ELALR at different current densities using a first-order model ($[F^-]_0$ = 15 mg/L, pH_i 7.4, κ = 2.4 mS/cm^2).

in agreement with those of Mameri et al. [14] and Emamjomeh and Sivakumar [18].

The first-order kinetics was also confirmed when the pH ranged between 2.86 and 10 in the ELALR [30,31]: the kinetic constant presented a maximum corresponding to a pH_i about 4 which agreed qualitatively with the data from Hu et al. 2007 [26]. Similarly, Mameri et al. [14] found an optimum pH_i around 5, whereas Shen et al. [16] indicated that the performance of defluoridation was maximized when the initial pH was close to 3. An additional difficulty with the analysis of the effect of pH_i is that the pH changes with time during EC and could either increase or decrease as a function of the pH_i [31]: experiments with a pH_i up to 7 lead to a pH increase, while pH exhibited a decrease vs. time when pH_i was higher than 8. This is due to the buffering effect of EC, as reported in [14,30,31,33] in which the optimum pH for $Al(OH)_3$ formation in the presence of fluoride anions was reported to lie between 5 and 7.

The first-order mechanism was also observed experimentally for various conductivity values in the ELALR. κ always decreased the cell voltage U at constant current density due to the decrease of the ohmic resistance of water [31], but it also decreased k_1 (data not presented). A first-order mechanism was always reported, but this was a pseudo-first-order mechanism, as k_1 depended on the initial fluoride concentration (Fig. 9), whereas k_1 should never depend on the initial concentration in a true first-order kinetics (Eq. (9)). Nevertheless, this result is quite common in the literature; for example, the evolution of k_1 with $[F^-]_0$ was quantified by Emamjomeh and

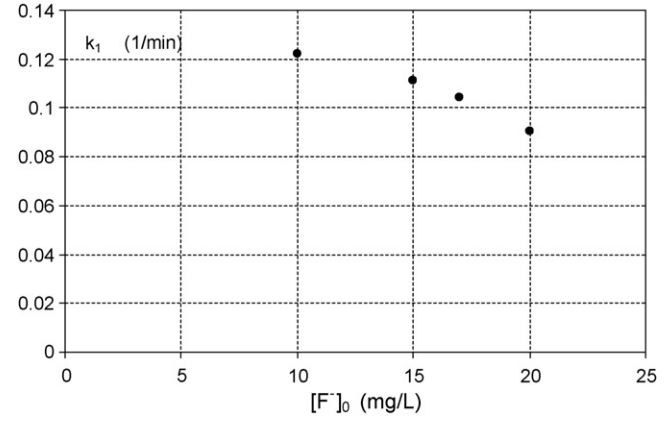

Fig. 9. Evolution of the kinetic constant k_1 of the first-order kinetic model in the ELALR as a function of the initial fluoride concentration (j = 17.1 mA/cm^2, pH_i 7.4, κ = 2.4 mS/cm^2).

Table 5
Estimation of the parameters of the statistical model described by Eq. (15) for K_{pred}.

Parameter	Estimate ($\times 10^3$)	Relative error (%)
a	−1.68	2
b	36.4	2
c	−12.6	5
d	−0.5	20
f	−7.61	3
g	250	9

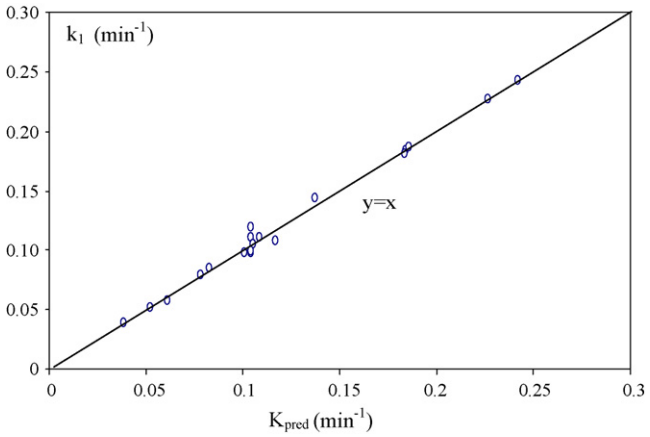

Fig. 10. Comparison between kinetic constant values deduced from experimental data (k_1) and predicted values (K_{pred}) using Eq. (16) for defluoradation by EC in the ELALR (j between 2.86 and 17.1 mA/cm^2, $[F^-]_0$ between 10 and 25 mg/L, pH_i between 4 and 10, κ between 2.4 and 20.5 mS/cm).

Sivakumar [18]. It should however be noted that the variation of k_1 with $[F^-]_0$ was smaller in this work (Fig. 9) than in [18].

As a result, a multiple regression analysis was developed to analyze the experimental data of the ELALR. The ranges of the main factors are as follows: j between 0 and 18 mA/cm^2; pH_i between 4 and 10; κ between 2.4 and 18 mS/cm. Several empirical models were confronted to the experimental results in order to find a mathematical expression which fits adequately the data with a minimum of adjustable parameters. The best model representing accurately the main trends can be written as follows:

$$K_{pred} = a \cdot j^2 + b \cdot j + c \cdot pH_i + d \cdot [F^-]_0^2 + f \cdot \kappa + g \quad (15)$$

In this expression, K_{pred} is the predicted value of k_1. Table 5 summarizes the estimation of the parameters and the relative error on their estimations; these parameters provide a determination coefficient R^2 = 0.982. This leads to the following expression:

$$K_{pred} = 10^{-3} \cdot [-1.68j^2 + 36.4j - 12.6pH_i - 0.5[F^-]_0^2 - 7.61\kappa + 250] \quad (16)$$

Thus, the retention time (t_N) to achieve a desired $[F^-]$ value can be deduced using the following relation:

$$t_N = \frac{10^3 \cdot \mathrm{Ln}([F^-]_0/[F^-])}{1.68 \cdot j^2 - 36.4 \cdot j - 12.6 \cdot pH_i - 0.5 \cdot [F^-]_0^2 - 7.61 \cdot \kappa + 250} \quad (17)$$

The comparison between the experimental values of k_1 and those of the predicted K_{pred} values resulting from the statistical model is illustrated in Fig. 10. This shows a very good agreement between experiments and simulations. Table 5 confirms that the predictions of k_1 decrease almost linearly with κ and with pH_i between 4 and 10, but also non-linearly with $[F^-]_0$, in agreement

with Fig. 10. For $[F^-]_0$ in the ELALR, this behaviour is in qualitative agreement with that observed in Section 3.3.1.2 for the STR: an increase of $[F^-]_0$ contributes to slow down the removal rate of fluoride. Table 5 also confirms that k_1 presents an optimum value as a function of j, as a parabolic trend was deduced from Eq. (16): first, k_1 increased with j up to 11.4 mA/cm^2, i.e. with the rate of aluminium released in the reactor; above this value, this rate was no more the limiting step of defluoridation, as in Section 3.3.1.1 for the STR, which explains that one deviates from the linear increase.

As a conclusion, the same trends are observed in the STR and the ELALR, but with different kinetics. As mentioned in [31], the fluoride removal is faster in the STR at the beginning of EC because mass transfer is not the limiting step when stirring speed is higher than 200 rpm: thus, the VOK model applies. In the ELALR, mixing is probably the limiting step because it cannot be controlled independently from current. This is in favour of a pseudo-first-order kinetics that can be modelled only using an empirical approach, as it follows qualitatively the same trends as the VOK model, but with an additional limitation due to mixing and mass transfer. This highlights that the pseudo-first-order kinetics, commonly encountered in the literature, results mainly from the poor mixing effectiveness of most laboratory EC cells and from the intrinsic adsorption capacity of aluminium electrodes [17]. Conversely, the chemical and electrochemical steps of EC can only be simulated using the VOK approach, as the limiting step seems to be the adsorption capacity of the adsorbent at the beginning of EC for good mixing conditions, especially when the S/V ratio is low in the EC reactor.

4. Conclusions

A kinetic study of defluoridation of drinking water was carried out using the electrocoagulation/electroflotation process in two batch reactors of identical volume (20 L): a stirred tank reactor (STR) and an external-loop airlift reactor (ELALR). The analysis of defluoridation operation revealed that once the external mass transfer was not limiting in the STR, the defluoridation kinetics could be simulated using the variable-order-kinetic approach (VOK) coupled with Langmuir–Freundlich adsorption isotherm. The adjusted parameters of this model were nearly independent of j and only slightly dependent of the initial fluoride content, as expected. A comparison with the adsorption isotherm of fluoride anions on already formed $Al(OH)_3$ flocs demonstrated the superiority of EC operation over conventional adsorption: fluoride anions are progressively incorporated into the flocs in EC, which increases drastically the adsorption capacity of insoluble aluminium hydroxides for removing fluoride anions.

Conversely, when mixing was less efficient, which is the case in the ELALR, experimental data could be fitted adequately only using a pseudo-first-order model. This constitutes, however, only an empirical approach based on a lumped parameter that accounts simultaneously for mass transfer, adsorption and electrochemical steps. In this case, only regression analysis could be used to establish a quantitative relationship between the kinetic constant and the operating conditions, such as current density and initial fluoride concentration. This highlights that the pseudo-first-order kinetics, mainly encountered in the literature, results mainly from the poor mixing effectiveness of most laboratory EC cells which are commonly operated at high current and S/V ratio, but only with magnetic stirring. As a result, the VOK model probably better represents the chemical and electrochemical steps of the EC process.

References

[1] World Health Organization, WHO Guidelines for Drinking Water Quality, World Health Organization, Geneva, 1993.
[2] C.Y. Hu, S.L. Lo, W.H. Kuan, Effects of the molar ratio of hydroxide and fluoride to Al(III) on fluoride removal by coagulation and electrocoagulation, J. Colloids Interface Sci. 283 (2005) 472–476.
[3] G. Singh, B. Kumar, P.K. Sen, J. Majumdar, Removal of fluoride from spent pot liner leachate using ion exchange, Water Environ. Res. 71 (1999) 36–42.
[4] N.I. Chubar, V.F. Samanidou, V.S. Kouts, G.G. Gallios, V.A. Kanibolotsky, V.V. Strelko, I.Z. Zhuravlev, Adsorption of fluoride, chloride, bromide, and bromate ions on a novel ion exchanger, J. Colloids Interface Sci. 291 (2005) 67–74.
[5] C. Castel, M. Schweizer, M.O. Simonnot, M. Sardin, Selective removal of fluoride ions by a two-way ion-exchange cyclic process, Chem. Eng. Sci. 55 (2000) 3341–3352.
[6] H. Lounici, L. Addour, D. Belhocine, H. Grib, S. Nicolas, B. Bariou, N. Mameri, Study of a new technique for fluoride removal from water, Desalination 114 (1997) 241–251.
[7] X. Fan, D.J. Parker, M.D. Smith, Adsorption kinetics of fluoride on low cost materials, Water Res. 37 (2003) 4929–4937.
[8] G.V. Kumar, I. Ali, V.K. Saini, Defluoridation of wastewaters using waste carbon slurry, Water Res. 41 (2007) 3307–3316.
[9] R.C. Meenakshi, Maheshwari, Fluoride in drinking water and its removal, J. Hazard. Mater. B 137 (2006) 456–463.
[10] Z. Amor, S. Malki, M. Taky, B. Bariou, N. Mameri, A. Elmidaoui, Optimization of fluoride removal from brackish water by electrodialysis, Desalination 120 (1998) 263–271.
[11] Z. Amor, B. Bariou, N. Mameri, M. Taky, S. Nicolas, A. Elmidaoui, Fluoride removal from brackish water by electrodialysis, Desalination 133 (2001) 215–223.
[12] D. Cohen, H.M. Conrad, 65,000 GPD fluoride removal membrane system in Lakeland, California, Desalination 117 (1998) 19–35.
[13] C.Y. Hu, S.L. Lo, W.H. Kuan, Effects of co-existing anions on fluoride removal in electrocoagulation (EC) process using aluminum electrodes, Water Res. 37 (2003) 4513–4523.
[14] N. Mameri, A.R. Yeddou, H. Lounici, D. Belhocine, H. Grib, B. Bariou, Defluoridation of septentrional Sahara water of north Africa by electrocoagulation process using bipolar aluminium electrodes, Water Res. 32 (1998) 1604–1612.
[15] N. Mameri, H. Lounici, D. Belhocine, H. Grib, D.L. Piron, Y. Yahiat, Defluoridation of Sahara water by small plant electrocoagulation using bipolar aluminium electrodes, Sep. Purif. Technol. 24 (2001) 113–119.
[16] F. Shen, X. Chen, P. Gao, G. Chen, Electrochemical removal of fluoride ions from industrial wastewater, Chem. Eng. Sci. 58 (2003) 987–993.
[17] J. Zhu, H. Zhao, J. Ni, Fluoride distribution in electrocoagulation defluoridation process, Sep. Purif. Technol. 56 (2007) 184–191.
[18] M.M. Emamjomeh, M. Sivakumar, An empirical model for defluoridation by batch monopolar electrocoagulation/flotation (ECF) process, J. Hazard. Mater. 131 (2006) 118–125.
[19] M.Y.A. Mollah, R. Schennach, J.R. Parga, D.L. Cocke, Electrocoagulation, (EC) – science and applications, J. Hazard. Mater. 84 (2001) 29–41.
[20] H.K. Hansen, P. Nunez, D. Raboy, I. Schippacasse, R. Grandon, Electrocoagulation in wastewater containing arsenic: comparing different process, Electrochim. Acta 52 (2007) 3464–3470.
[21] N. Daneshvar, H.A. Sorkhabi, M.B. Kasiri, Decolorization of dye solution containing Acid Red 14 by electrocoagulation with a comparative investigation of different electrode connections, J. Hazard. Mater. B 112 (2004) 55–62.
[22] M. Kobya, O.T. Can, M. Bayramoglu, Treatment of textile wastewaters by electrocoagulation using iron and aluminium electrodes, J. Hazard. Mater. 100 (2003) 163–178.
[23] M. Bayramoglu, M. Eyvaz, M. Kobya, Treatment of the textile wastewater by electrocoagulation: economical evaluation, Chem. Eng. J. 128 (2007) 155–161.
[24] M.Y.A. Mollah, P. Morkovsky, J.A.G. Gomes, M. Kesmez, J.R. Parga, D.L. Cocke, Fundamentals, present and future perspectives of electrocoagulation, J. Hazard. Mater. 114 (2004) 199–210.
[25] P.K. Holt, G.W. Barton, C.A. Mitchell, The future for electrocoagulation as a localised water treatment technology, Chemosphere 59 (2005) 355–367.
[26] C.Y. Hu, S.L. Lo, W.H. Kuan, Simulation the kinetics of fluoride removal by electrocoagulation (EC) process using aluminium electrodes, J. Hazard. Mater. 145 (2007) 180–185.
[27] Y. Chisti, Airlift Bioreactors, Elsevier, London, 1989, 355.
[28] A.H. Essadki, M. Bennajah, B. Gourich, Ch. Vial, M. Azzi, H. Delmas, Electrocoagulation/electroflotation in an external-loop airlift reactor—application to the decolorization of textile dye wastewater: a case study, Chem. Eng. Process. 47 (2008) 1211–1223.
[29] B. Merzouk, B. Gourich, A. Sekki, K. Madani, Ch. Vial, M. Barkaoui, Studies on the decolorization of textile dye wastewater by continuous electrocoagulation process, Chem. Eng. J. 149 (2009) 207–214.
[30] M. Bennajah, B. Gourich, A.H. Essadki, Ch. Vial, H. Delmas, Defluoridation of Morocco drinking water by electrocoagulation/electroflottation in an electrochemical external-loop airlift reactor, Chem. Eng. J. 148 (2009) 122–131.
[31] A.H. Essadki, B. Gourich, Ch. Vial, H. Delmas, M. Bennajah, Defluoridation of drinking water by electrocoagulation/electroflotation in a stirred tank reactor with a comparative performance to an external-loop airlift reactor, J. Hazard. Mater. 168 (2009) 1325–1333.
[32] S. Azizian, M. Haerifar, J. Basiri-Parsa, Extended geometric method: a simple approach to derive adsorption rate constants of Langmuir–Freundlich kinetics, Chemosphere 68 (2007) 2040–2046.
[33] D.H.F. Liu, B.G. Liptak, Wastewater Treatment, Lewis Publishers, Boca Raton, 2000, pp. 256–262.